A three-dimensional multi-electrode array for multi-site stimulation and recording in acute brain slices

Marc Olivier Heuschkel [a],*, Michael Fejtl [b], Mario Raggenbass [c], Daniel Bertrand [c], Philippe Renaud [a]

[a] *Institute of Microsystems, EPFL, CH-1015 Lausanne, Switzerland*
[b] *Multi Channel Systems, Markwiesenstr. 55, D-72770 Reutlingen, Germany*
[c] *Department of Physiology, CMU, Rue Michel-Servet 1, CH-1211 Geneva 4, Switzerland*

Abstract

Several multi-electrode array devices integrating planar metal electrodes were designed in the past 30 years for extracellular stimulation and recording from cultured neuronal cells and organotypic brain slices. However, these devices are not well suited for recordings from acute brain slice preparations due to a dead cell layer at the tissue slice border that appears during the cutting procedure. To overcome this problem, we propose the use of protruding 3D electrodes, i.e. tip-shaped electrodes, allowing tissue penetration in order to get closer to living neurons in the tissue slice. In this paper, we describe the design and fabrication of planar and 3D protruding multi-electrode arrays. The electrical differences between planar and 3D protruding electrode configuration were simulated and verified experimentally. Finally, a comparison between the planar and 3D protruding electrode configuration was realized by stimulation and recording from acute rat hippocampus slices. The results show that larger signal amplitudes in the millivolt range can be obtained with the 3D electrode devices. Spikes corresponding to single cell activity could be monitored in the hippocampus CA3 and CA1 region using 3D electrodes. © 2002 Elsevier Science B.V. All rights reserved.

Keywords: Multi-electrode array; Protruding electrodes; Tip-shaped electrodes; Simulation; Acute slice; Rat hippocampus; Electrical stimulation; Extracellular recording

1. Introduction

Ever since the introduction of planar multi-electrode arrays (MEA) to the neuroscience community by Thomas et al. (1972) and Gross et al. (1977), network activity of excitable cells has been studied with these devices. The majority of the recordings were applied to cell cultures and organotypic preparations. The advantage of cells cultured on a MEA is that it allows for the necessary time to establish a tight seal between the cell membrane and the electrode surface. However, the disadvantages of cell culture systems are: loss of synaptic arrangement, tissue modification, signal to noise is hampered, the cost and time to prepare and maintain the culture, the possibility of aberrant connections, contamination, and the like.

Earlier reports by Wheeler and Novak (1986) and Novak and Wheeler (1988, 1989) presented recordings from acute slices on planar MEA. Evoked epileptiform field potentials in the mV range were recorded in the rat hippocampus slices, the slice environments being similar to that in a standard interface chamber, which allows maximizing of the signal levels. It is well known that the amplitude is larger for slices recorded at the interface than those of slices recorded in immerged conditions. Another MEA used for acute slice preparations has been only recently described (Oka et al., 1999).

Electrode coupling, i.e. a tight seal resistance between the tissue and the electrodes is often difficult to achieve because of the dead cell layers present at the surface of

---

* Corresponding author. Present address: Ayanda Biosystems, Science Park, EPFL/PSE, CH-1015 Lausanne, Switzerland. Tel./fax: + 41-21-693-8631.

E-mail address: marc.heuschkel@ayanda-biosys.com (M.O. Heuschkel).

the slice, which are caused by the cutting procedure. Nevertheless, a few papers have described more or less stable recordings of excitatory post-synaptic potentials (EPSPs) and population spikes over several hours (Novak and Wheeler, 1988; Oka et al., 1999). When carefully looking at these data, it is observed that the amplitudes of evoked responses are an order of magnitude lower than responses obtained with conventional glass microelectrodes. Taking into account the existence of a dead cell layer, it is evident that the site of recording does not coincide with the site of origin of the signal. Most likely, the active cells producing EPSPs
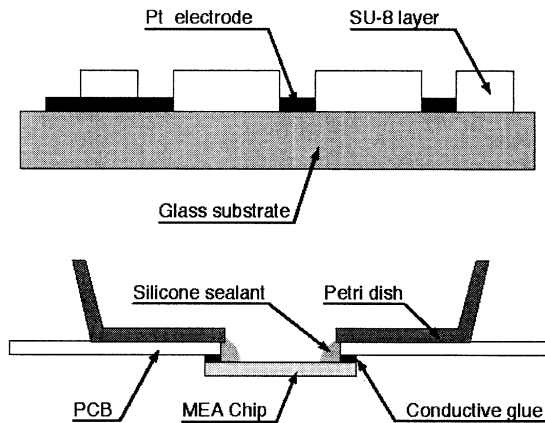

Fig. 1. Top, schematic cross-section of a multi-electrode array chip composed of a glass substrate, patterned platinum electrodes and an SU-8 epoxy insulation layer. Bottom, scheme of multi-electrode array (MEA) device backend assembly. The MEA chip is glued under a printed circuit board for signal output to external signal amplification and data acquisition. The bottom part of a Petri dish defines the culture chamber. A silicone sealant insures that the culture chamber remains watertight.
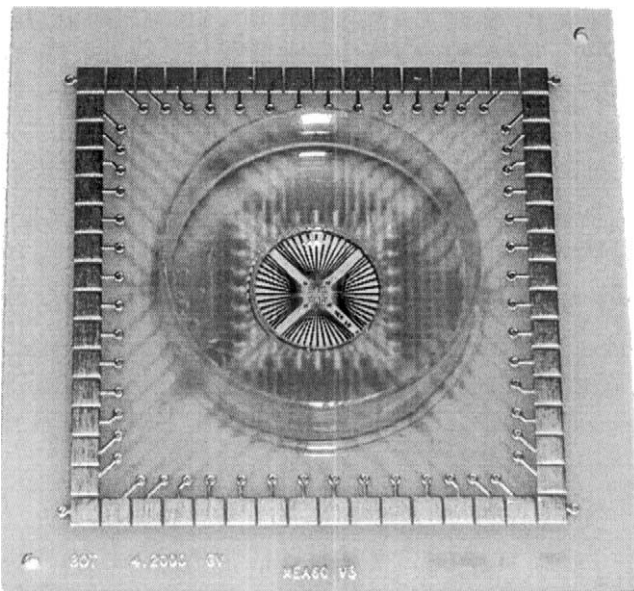

Fig. 2. Overview of a 60 electrode MEA device. External dimensions are 5×5 cm^2.

or spikes are at least one or two cell layers above the measuring electrodes of a conventional planar MEA.

A first attempt to achieve higher signal amplitudes with extracellular electrode arrays was made using a three-dimensional electrode approach. Protruding electrodes were fabricated by electrochemical deposition of platinum (Thiébaud et al., 1997) and wet chemical etching of bulk silicon (Thiébaud et al., 1999). However, no direct comparison between planar and tissue-penetrating electrodes was reported so far.

We present new 3D MEA based on glass substrates that are able to penetrate the dead cell layer(s) and record the ongoing extracellular activity from a site closer to its origin. We have simulated electrical characteristics of planar and 3D electrodes to evaluate the improvement of a tip-shaped 3D MEA. Finally, stimulation and recordings of neuronal activity in acute rat hippocampus slices were carried out with planar and 3D MEA. Our results show that larger amplitudes of evoked responses can be recorded with the new 3D MEA. Moreover, recorded signal amplitudes are in the millivolt range rather than being only ca. 0.18 mV as described by Oka et al. (1999), who used a conventional planar MEA. Thus, we suggest that these 3D MEA can serve as a new tool to more precisely unravel the neural network properties in acute brain slices.

2. Materials and methods

2.1. Multi-electrode arrays

Microelectronic fabrication technologies allow low-cost fabrication of microstructures by combining a small chip size with printed circuit boards for external connectivity. The MEA chips are fabricated under cleanroom conditions using standard photolithography, wet chemical etching and thin film deposition technologies (Madou, 1997; Rai-Choudhury, 1997). They are composed of a glass substrate, thin film platinum electrodes and a 5 μm thick SU-8 (Lorenz et al., 1997, 1998) epoxy insulation layer (Fig. 1 top). The MEA chips are then glued onto printed circuit boards by a screen-printing technique. The recording chamber is formed by the bottom part of a Petri dish in which a hole was stamped for access of the electrode array. Finally, the recording chamber is sealed with silicone to ensure watertight connection of the MEA (Fig. 1 bottom). It results in a 5×5 cm^2 large device that fits into an external data acquisition interface (Fig. 2).

An important improvement in our MEA concept is the connection of the chips to small printed circuit boards. In this way, the chip size is reduced, allowing an increase in number of chips that can be processed on one single glass substrate and thus a reduction of the overall cost per chip. On the other hand, the obtained
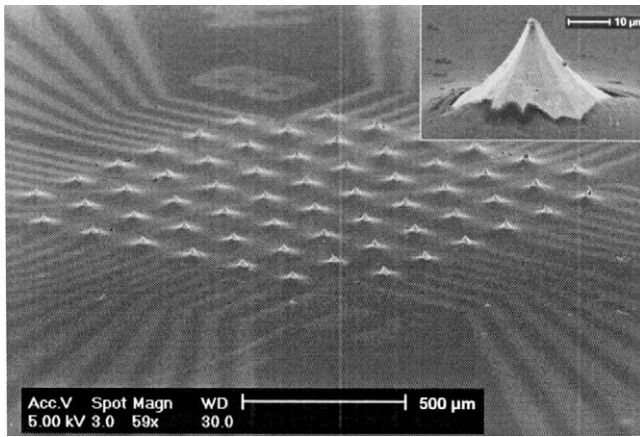
Fig. 3. SEM picture of 3D MEA recording area. It is composed of 60 tip-shaped protruding platinum electrodes. The height of the glass tips is about 60 μm, however, only 40 μm at the top of the tips form the effective recording electrodes. A thin epoxy layer insulates the electrode leads.

chips have to be released by substrate dicing and to be mounted onto a printed circuit board. However, these supplementary fabrication steps are low-cost compared to the chip microfabrication process. Another advantage of this fabrication concept is that different device layouts can be easily accomplished.

Our planar and 3D MEA designs are composed of 60 electrodes arranged in an 8×8 matrix without corner electrodes. The electrodes are 40×40 μm² squares spaced by 200 μm (center to center) defining a recording area of about 1.4×1.4 mm² in the center of the microchip.

In the 3D MEA configuration, 60 μm high glass tips are etched at the glass substrate surface. The top of these tips is then covered with the electrodes, however, only 40 μm at the top of the glass tips form the effective recording area (Fig. 3)[1].

2.2. Simulations

In order to simulate the electrical field between a cell in a tissue slice and an underlying electrode, we used a finite element model in FEMLAB® simulation program (Comsol AB, Stockholm, Sweden). The physical model used in FEMLAB® is a two dimensional DC conductive media model, based on a relation relating the current density J to the electrical field E:

$$J = \sigma E. \tag{1}$$

Combining the continuity equation:

$$\nabla \cdot J = Q, \tag{2}$$

where Q is a current source, with the definition of the electrical potential V yields the elliptic Poisson's equation defined as:

$$Q = -\nabla \cdot (\sigma \nabla V). \tag{3}$$

The two only resulting parameters are the conductivity σ and the current source Q, which is always equal to zero in our model. Dirichlet and Neumann boundary conditions were assigned to the model. The Dirichlet boundary condition assigns values of the electric potential V to the boundaries. The Neumann boundary condition requires the value of the normal component of the current density $\mathbf{n} \cdot (\sigma \nabla V)$ to be known and is defined by $\mathbf{n} \cdot (\sigma \nabla V) + qV = g$, where q can be interpreted as the film conductance for thin plates and g is the current (always equal to zero in our model). The film conductance q equals to the inverse of the film resistance, i.e. the inverse of the electrode resistance.

Two simple geometrical models were simulated to estimate the difference between planar and 3D electrodes while monitoring biological activity in tissue slices. For computational simplicity, we have used a 2D electrical model that reduces the element geometry but still remains a valid model for comparison of electrical characteristics of a planar versus a tip-shaped MEA.

2.2.1. Signal magnitude simulation in case of a locally fixed cell

The simulation of the electrode signal magnitude for different electrode shapes (planar and 3D electrodes with a tip height up to 80 μm) was made assuming a biological signal source above the recording electrode at a fixed position (see Fig. 6 top).

A spherical cell soma with a diameter of 20 μm (circle) and an axon (rectangle) of a diameter of 1 μm and an infinite length model the signal source (Rall, 1962). The cell soma is located next to the planar electrode border, 60 μm above the substrate level. The simulated voltage at the cell surface is applied to the border conditions of the modeled cell (-60 mV at the soma and 40 mV at the axon). The dead cell layers in between this active cell and the electrode, are assumed to be a resistive homogeneous media, its conductivity being equal to saline solution.

The planar electrodes are modeled by a square electrode with dimension of 40×40 μm² (40 μm long line at substrate level). On the other hand, the 3D electrodes are modeled by a conical electrode shape with a tip height varying from 20 up to 80 μm, the top of the tip being the effective electrode (2/3 of tip height). Neumann boundary conditions were applied to the electrodes: $g = 0$, and q being the inverse of the electrode resistance per μm² multiplied by the geometric length of the modeled electrode. To take into account the electrode surface difference between the planar and 3D electrodes and the resulting electrical properties, the 3D

---

[1] To obtain the 3D MEA please contact Multi Channel Systems (www.multichannelsystems.com).

electrode boundary conditions were defined as $g = 0$ and q being the inverse of the electrode resistance per μm^2 multiplied by the geometric length of the modeled electrode and the electrode surface ratio between the 3D and the planar electrode.

The electrodes are connected by a lead to the ground. This electrode lead is modeled between the glass substrate and the insulation layer at the left side of the electrode. Finally, the glass substrate and the insulation layer are modeled to be high resistive material ($g = 0$, $q = 0$).

2.2.2. Simulation of recorded signal versus the signal source location

This simulation was achieved by modeling the measurement electrode, i.e. a planar and a 60 μm high tip-shaped 3D electrode (as described before), and a signal source located at different heights above the center of the electrode (see Fig. 7 top).

The signal source used in this model was modeled as a circle (diameter of 20 μm) divided into two parts representing an electrical dipole of 100 mV. The electrical dipole was applied to the signal source border conditions (100 mV left side, 0 V right side). The source was located over the center of the electrode and also at different positions beside the electrode, at a substrate level/source height varying between 0 and 300 μm. The space in between the dipole and the electrode was assigned to be a resistive homogeneous media with conductivity equal to saline solution, which simplifies the model and can also be reproduced experimentally with a theta glass pipette electrode.

2.3. Preparation of acute hippocampal slices

Experiments were carried out with young male rats (ca. 3–4 weeks old, 120–150 g) of the Sprague–Dawley strain. The animals were sacrificed by decapitation. Anesthesia was avoided, since most anesthetics do obviously affect the brain and its efficacy depends strongly on the weight of the animal. Animal handling and preparation was carried out according to the animal rights Swiss ethical rules.

The brain was quickly removed and put into ice-cold (4 °C) artificial cerebrospinal fluid (ACSF composition in mM: NaCl 135, KCl 5, $NaHCO_3$ 15, $MgCl_2$ 1 and glucose 10; pH 7.4). Calcium was omitted in order to prevent excitatory synaptic transmission during the cutting procedure. Transverse hippocampal slices (350 μm thickness) were cut with a vibrating tissue chopper. The slices were then pre-incubated at room temperature in ACSF containing 2 mM $CaCl_2$, and gassed with 95% O_2/5% CO_2, for at least 1 h.

To improve tissue adhesion, the electrode array was pre-coated with 0.1% polyethylenimine (PEI) for 2 h, extensively rinsed with distilled water and allowed to dry. The slices were then placed onto pre-coated and dry MEA and positioned over the electrode matrix. After positioning of the slice, the surrounding solution was removed with a pipette. The remaining solution between the slice and the MEA surface was removed with tissue paper. Fresh ACSF solution was quickly introduced in the dish on top of the slice. The MEA was then transferred to a MEA1060 amplifier interface (Multi Channel Systems GmbH, Germany) and the preparation continuously perfused (2–3 ml/min) during the recording session.

2.4. Electrophysiological recordings

Slices were stimulated with monopolar current pulses applied between one of the electrodes and a reference Ag/AgCl wire, and voltage responses were monitored at the 59 remaining electrodes. To construct an input/output (I/O) curve, we used biphasic current pulses ($-/+$ pulses lasting 120 μs) ranging from 0 to 360 μA in 30 μA steps. Thus, 12 values were used to construct the I/O curve. We observed that the negative flank of a pulse yielded the smallest artifact while providing best stimulation.

Three responses with an inter-spike interval of 2 s were collected for each stimulation step. I/O curves were consecutively measured at least three times every 10 min. The first 15 min were reserved for selecting a stimulation electrode and establishing the steady-state condition.

We stimulated Schaffer collateral axons in the CA1 region or at the CA3/CA1 border and measured the evoked responses at the pyramidal cell layer in the CA1 region. Alternatively, we stimulated the dentate gyrus, which generates evoked responses in CA3 region via the mossy fiber pathway.

3. Results and discussion

3.1. Electrical characteristics of planar and 3D MEA

In order to compare planar electrodes with 3D electrodes, the electrical properties of both were estimated by measuring the impedance and phase shift versus frequency, by sweeping the frequency from 100 Hz to 20 kHz. The electrode resistance and the electrode capacitance were then calculated. Note that the resistance is inversely proportional to the area and the interface capacitance is directly proportional to it.

In the 3D arrays, there is a difference in electrode impedance due to an increase of the geometrical electrode surface. The effective 3D electrode area can be approximated by the lateral surface of a cone (underestimation) or of a pyramid (overestimation) with a basis of 40 μm and a height of 40 μm. This yields an

electrode surface between 2809 and 3600 μm^2, respectively. Comparing this value to a planar electrode surface of 1600 μm^2, there is an electrode surface increase of a factor between 1.75 and 2.25.

The measured impedance value of the planar electrode is 2.08 times higher than the 3D electrode impedance, which corresponds roughly to the electrode area increase (Fig. 4 top). However, the phase shift yielded similar values in both measurements (Fig. 4 bottom). The resulting value of the global electrode resistance for the 3D MEA electrodes is 2.14 times smaller and the global electrode capacitance is 2.08 times larger than for planar electrodes (Fig. 5).

The electrode noise is mainly due to the electrode's thermal noise defined by:

$$U\text{th} = \sqrt{4\ kTRB},$$

where k is the Boltzmann constant, T is the temperature, R is the global resistance of the electrode and B is the electrode bandwidth. According to this equation,
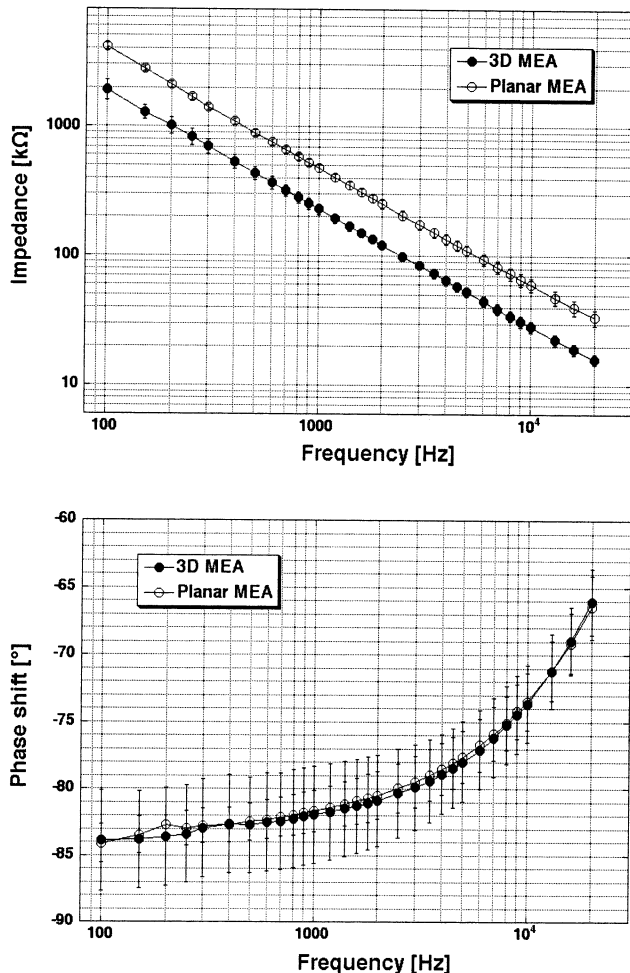

Fig. 4. Measured impedance Z (top) and phase shift θ (bottom) versus frequency for planar and 3D MEA in a 0.9% NaCl solution. A 100 mV, 100 kHz AC voltage signal was applied to the electrodes during these measurements.
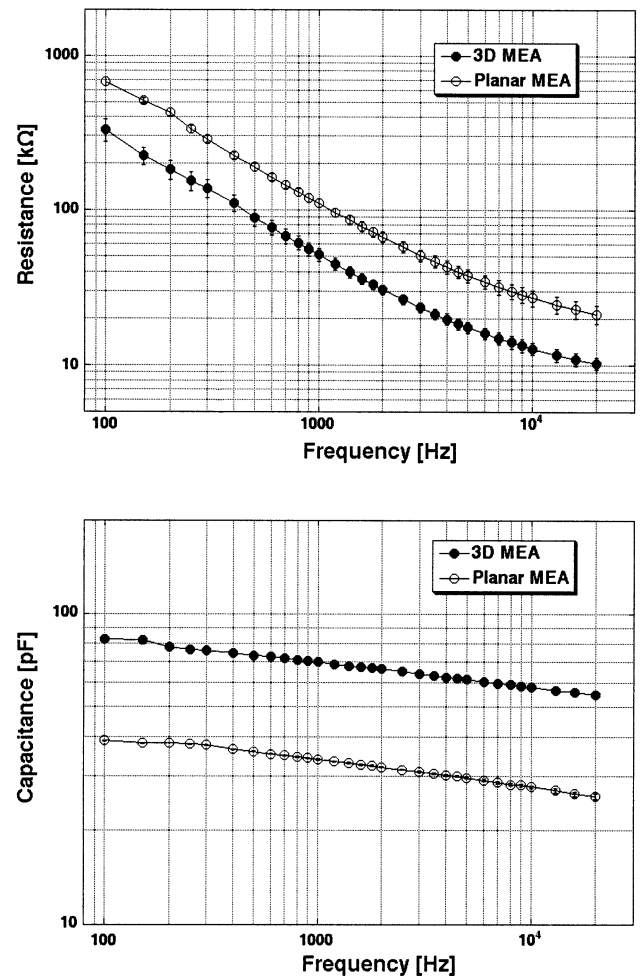

Fig. 5. Using the data from Fig. 4, the global electrode resistance (top) and capacitance (bottom) were calculated for both the planar and 3D electrodes versus frequency. The resistance is defined as $R = Z\cos(\theta)$ and the capacitance is defined as $1/C = (2\pi F)\ Z\sin(\theta)$, where F is the frequency. Due to an increased electrode area, the 3D electrodes show a lower resistance and a larger capacitance than planar electrodes.

there should be a noise reduction of a factor 1.44 for the 3D electrode due to its proportionality to the square root of the electrode resistance. The measured noise levels show a reduction from 20–25 μV for planar electrodes to 14–17 μV for 3D electrodes, which corresponds to a decrease of a factor between 1.17 and 1.78. The result is that the signal-to-noise ratio is increased for a given signal amplitude due to the electrode geometry variation (larger electrode area). However, the signal-to-noise ratio is dependent on the signal amplitude, which also varies with the electrode configuration.

The larger capacitance of the 3D electrodes results in a higher safe-charge-injection limit. This is important for cell or tissue stimulation through the 3D electrodes because more electrical charge can be applied through the electrode before irreversible electrolysis, i.e. ohmic current flow occurs.
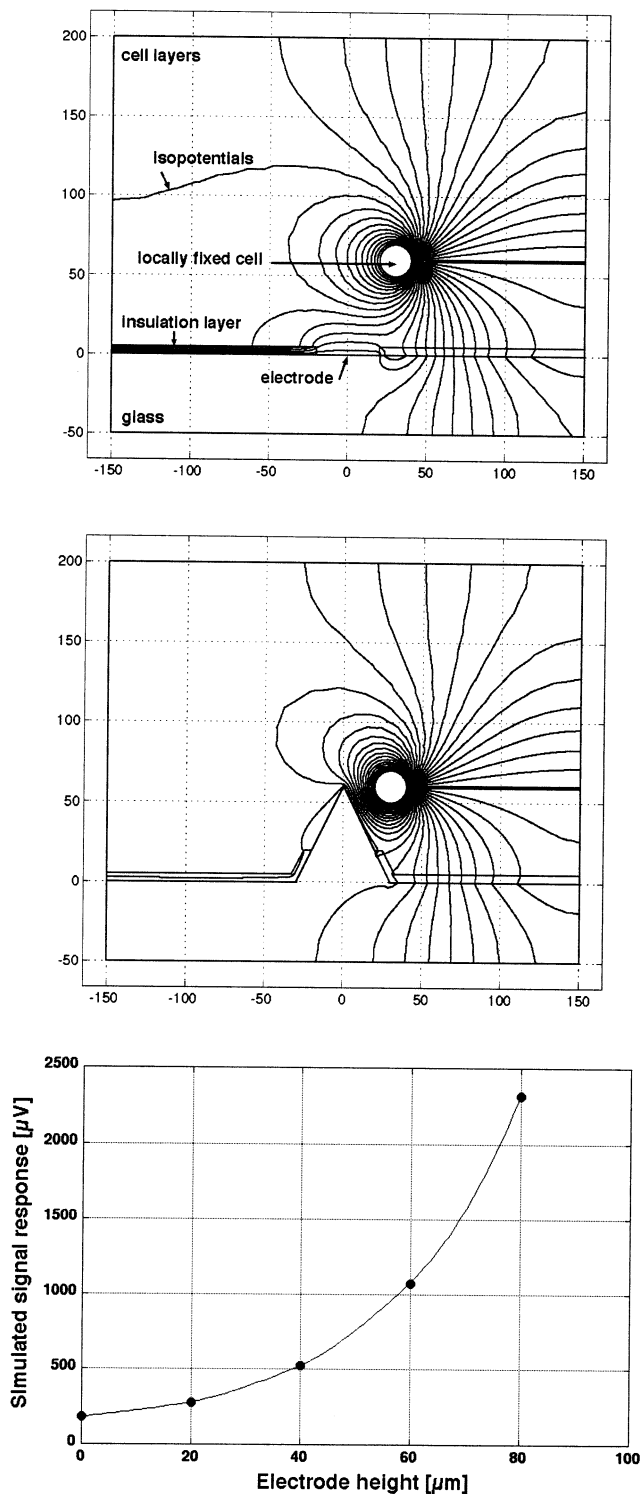
3.2. Simulation of 3D versus planar electrode configuration

The rationale for using tip-shaped electrodes for acute slice recordings was to get closer to the active cells, and thereby to improve the electrical measurement and stimulation conditions. Dead cell layers always remain at the border of tissue slices when cutting slices with a vibrating tissue chopper, and therefore, the first layer of electrically active cells is estimated to be at about 50 μm inside the tissue.

Our main goal was to record the electrical activity in the vicinity of active neurons by penetrating the slice. By changing the electrode geometry, the measurement condition improvement is due to the shorter distance between the electrodes and the active cells in the slice. The electrical field generated by the de- or hyperpolarization of the cell membrane is sensed with the extracellular measuring electrodes. The strength of the electrical field decreases with the square of the distance, and hence, the measured signal amplitude should increase when 3D electrodes are used. In addition, 3D electrodes should improve electrical stimulation by shifting the input/output relation (I/O-curve) to lower stimulation currents. Indeed, a more local stimulation due to the tip geometry and a shorter distance between the electrodes and the cells should improve the stimulation of the cells. Thus a distinct response level should be reached with less current than in a planar electrode configuration. This will also lead to a longer lifetime of the 3D MEA, since degradation of the active tip electrode depends on the overall current strength used for stimulation.

3.2.1. Signal magnitude simulation in the case of a locally fixed cell

The simulation results shown in Fig. 6 indicate that larger recorded signal amplitudes should be achieved with 3D electrodes. However, the measurable signal amplitudes are due to a combination of two effects in this simulation: the increase of the electrode surface with the increase of the electrode height, and the effect of the 3D electrode geometry getting closer to the cell. When comparing the signal amplitude of a planar and a 3D electrode with a tip height of 60 μm, the amplitude rises with a factor close to 5.8. While this simulation model does not take into account a displacement of the cell when using a 3D electrode (ideal tissue penetration), this would certainly not be achieved in real experiments. Experimental measurements using acute hippocampal slices in both these configurations will be described below. Furthermore, the results suggest that higher electrodes should enhance the signal.
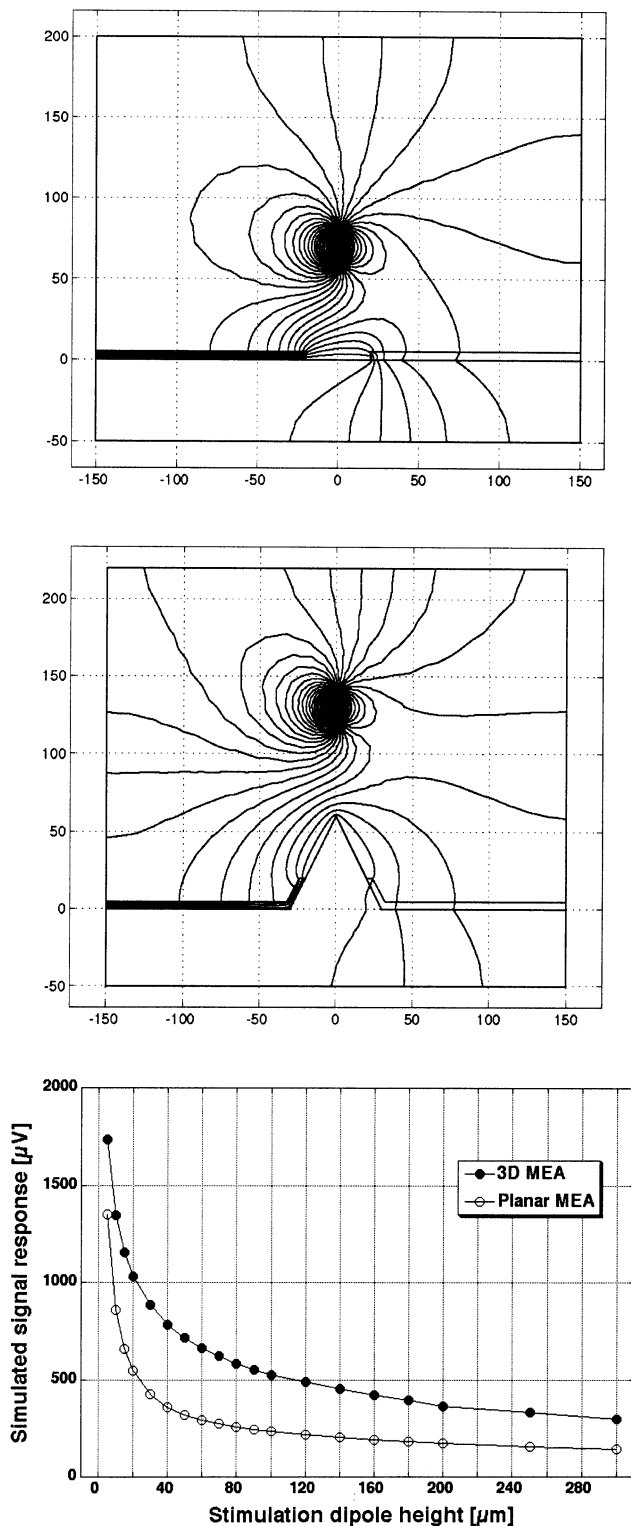

Fig. 6. Top, simulation of isopotentials in the case of a single cell signal source (− 60 mV at the soma and 40 mV at the axon), for both a planar and a 3D electrode (tip height of 60 μm, the electrode covers about 40 μm at the top of the tip), located 60 μm above the substrate at the electrode border. The scales represent the geometrical dimensions in μm. The potential difference between two isopotentials is 4 mV. Bottom, plot of the signal amplitude versus electrode tip heights, the 0 μm height corresponding to a planar electrode. The measurable signal response increases with the height of the electrode due to an electrode area increase and the lower distance between the cell and the electrode.

Fig. 7. Top, simulation of isopotentials in the case of both a planar and a 3D (tip height of 60 μm, the electrode covers about 40 μm at the top of the tip) electrode configuration for an electrical dipole of 100 mV located above the center of the electrode moving along the *z*-axis. The dipole is modeled by a circle, the left side being at 100 mV and the right side being at 0 V. The scales represent the geometrical dimensions in μm. Bottom, plot of the resulting electrode potential in both cases versus the distance between the electrode and the dipole. The shift between both traces is due to the electrode surface increase of the 3D electrode. The geometry of the electrode does not play a role in this configuration.

3.2.2. Simulation of recorded signal versus the signal source location

The simulation results in Fig. 7 show that the signal amplitude decreases with the square of the distance between the electrode and the signal source, when the source is located above the center of the electrode. In this configuration, there is no geometrical advantage when using 3D electrodes, but rather an advantage for the planar electrodes when the electrode/signal source distance is small. The shape of the traces obtained by this simulation is almost the same. The only observable difference of these simulation results is a shift to larger amplitudes for the 3D electrodes, which is due to the different electrode characteristics. To control this assumption, the electrode characteristics of the planar electrode model were modified to be equivalent to the 3D electrode characteristics, and the resulting simulation trace roughly superimpose the 3D electrode trace (data not shown).

However, geometrical effects can be simulated when moving the position of the signal source beside the recording electrode. It was chosen to locate the signal source center at 40, 65, 90, and 140 μm beside the electrode center (*x*-axis) at heights between 5 and 300 μm above the substrate level (*z*-axis). The resulting simulations in Fig. 8 show that the 3D electrode configuration provides a larger signal due to a shorter distance between the electrode and the source when the signal source is close to the electrode location (small *x* value). This is especially the case when the source lies between 20 and 80 μm above the substrate, which corresponds to the first active cell layer(s) in an acute tissue slice.

As the real experimental case was simulated, the traces of the planar electrode configuration are shifted to lower amplitudes due to the electrode surface difference between the two electrodes. When using the same electrode characteristics in both cases, the planar electrode traces are superimposed at large electrode/signal source distances, especially for *z* values larger than 200 μm (data not shown).

3.3. Verification of the simulations

To experimentally verify the potential variation measured by the electrode in the presence of a source simulating a cell located at different heights over or next to the electrode for both planar and 3D electrodes, an experiment using a theta glass pipette electrode was employed. This experiment was designed to measure the potential detected by a planar and a 3D electrode when a dipole was located and moved above the substrate beside or above the center of the electrodes.

The picture in Fig. 9a shows the employed glass pipette with an aperture of 20 μm over planar MEA electrodes. When biphasic potential pulses (− / +) of

100 mV, 2 ms were applied, a signal could be measured on all electrodes of the MEA as shown in Fig. 9b. This experiment illustrates the decrease of the electrical field generated by the glass pipette in the solution as a function of distance in the x- and y-axes. Fig. 9c shows a plot of the recorded potentials obtained along the x-axis during this experiment as a function of the distance between the stimulation and the recording electrodes, whereby the stimulation electrode was located above one electrode at the border of the electrode array. The recordings show a good correlation with the simulation results shown in Fig. 7c, demonstrating that the simulations illustrate well the reality.

Measurements obtained with both planar and 3D electrodes versus the electrode/signal source distance (z-axis) above the center of the electrode were plotted in Fig. 9d. When comparing the experimental results with the simulations shown in Fig. 7c, it seems that the experimental results correspond to simulated values shifted to larger values in the z-axis (about 20–30 μm). This can be explained by the difficulty to evaluate exactly the distance between the electrode and the theta microelectrode during the experiment. Note also the amplitude difference between the two electrode configurations due to the electrode surface difference.

Experiments with the signal source close beside the electrodes were more difficult to realize, especially when using 3D electrodes due to the shape of the

bottom part of the electrodes. Fig. 9e shows the advantage of the 3D electrode's geometry. The position of the signal source centered on the x-axis was about 60 μm for both electrode configurations. The results obtained using the planar electrode arrays correspond roughly to the simulations shown in Fig. 8. On the other hand, the amplitude obtained using the 3D electrodes was lower than in the simulations. The height of the electrode array glass tips used for these simulation verifications was 60 μm, however, only 30 μm at the top of the tip corresponded to the effective electrode, which also explains lower amplitude responses due to smaller electrodes used in experiment than in the simulations.

3.4. Single unit recordings of spontaneous activity

Recordings using the planar and 3D electrodes were made on acute rat hippocampal slices. One possible solution to maintain the slice in a steady position is to use a nylon mesh (Fig. 10 top). Improvement of cell contact with the MEA was observed by recording of spontaneous activity that closely resembles that of a single cell. Under these conditions, spontaneous single action potentials could be recorded from electrodes located under pyramidal neurons of CA3 and CA1 region, especially when a nylon line lay directly next to or above the electrode. Signal amplitudes up to 80 μV

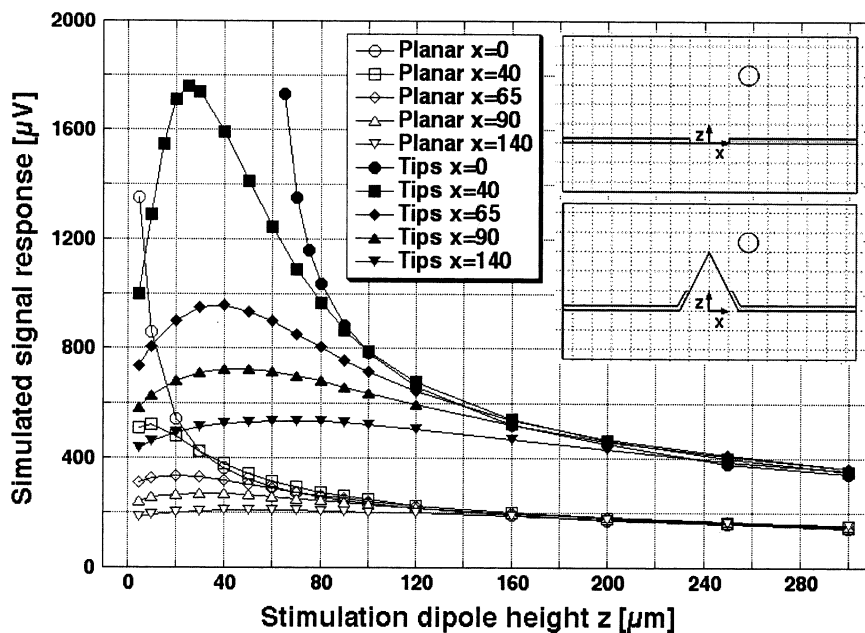Fig. 8. Electrode potential simulations in the case of both a planar and a 3D (tip height of 60 μm) electrode configuration for an electrical dipole of 100 mV moving along the z-axis above the substrate at different x-axis locations. The dipole is modeled by a circle, the left side being at 100 mV and the right side being at 0 V. Results show the advantage of the 3D electrode geometry against the planar electrode when a cell is located close to an electrode site. The amplitude shift between the two traces is mainly due to the different electrode characteristics due to the 3D electrode surface increase.
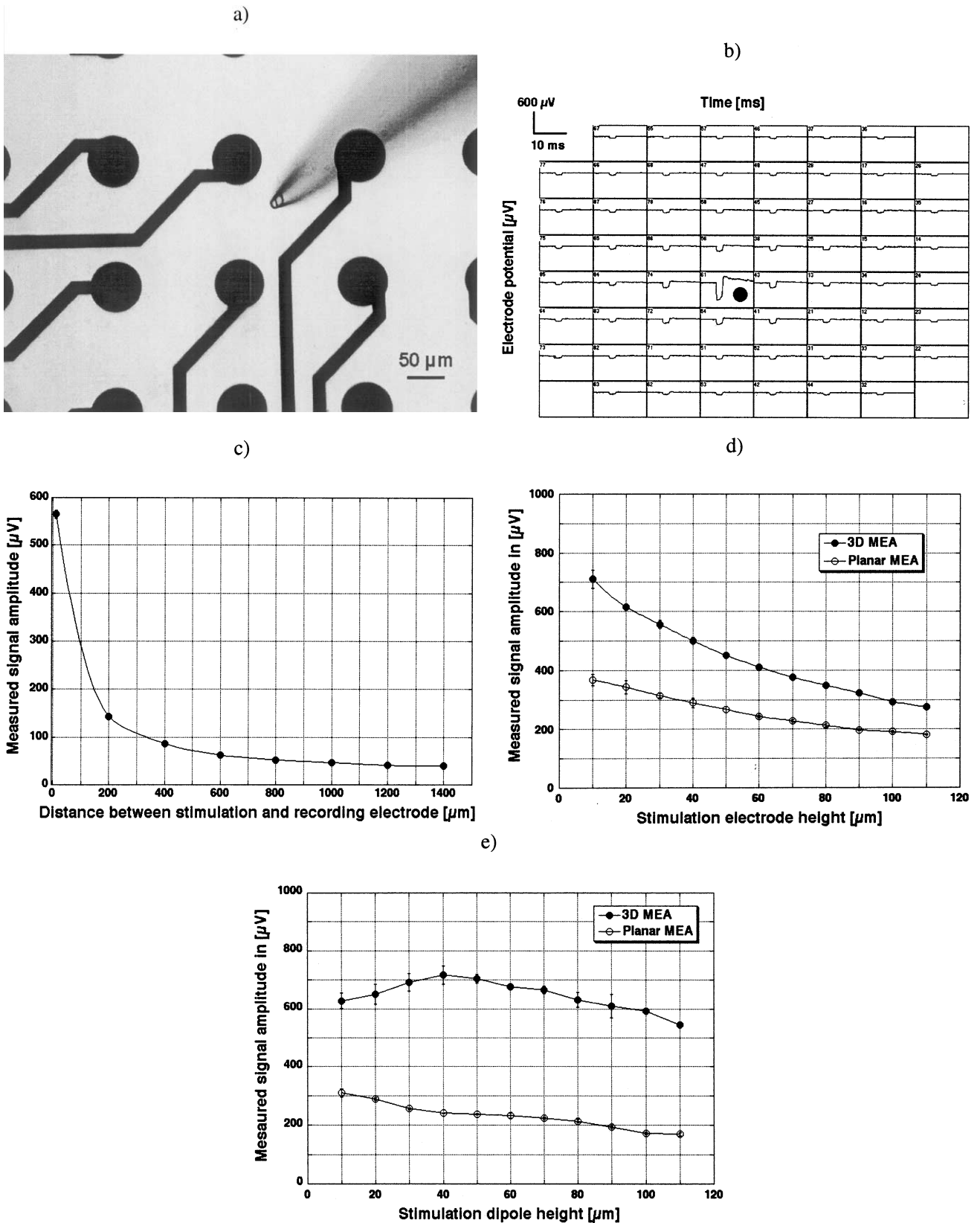
Fig. 9. (a) Picture of a theta glass pipette electrode used as a potential dipole source shown above planar MEA electrodes. (b) Plot of the MEA response to a 100 mV pulse applied above one planar electrode (black dot). Each square represents the signal from one electrode. The measured signal amplitude decreases with the distance (200 μm between two electrodes). (c) Plot of the potential versus electrode/source distance in a similar configuration than shown in (b). (d) Resulting plot of potential measurement for both planar and 3D electrodes versus location of the dipole located above the electrode center. It appears that the obtained results are shifted in the *z*-axis when compared to the simulation results obtained in Fig. 7, which can be explained by the bad theta glass electrode height control during experiments. (e) Resulting plot of potential measurement for both planar and 3D electrodes versus location of the dipole located beside the electrode. The obtained results correspond roughly to the simulation shown in Fig. 8 (see text).

could be obtained using 3D electrode arrays (Fig. 10 bottom).

3.5. Recording of evoked field excitatory post-synaptic potentials and population spikes

The simulation of the effect of 3D protruding electrodes versus planar electrodes was verified in physiological recordings from acute hippocampal slices. Schaffer collateral axons were stimulated in the CA3/CA1 or CA1 region, and evoked field excitatory post-synaptic potentials (fEPSP) and large population spike responses were measured in the CA1 region, in the dendritic and pyramidal cell layer, respectively. The amplitudes of measured extracellular responses fluctuate from a few hundreds μV to more than one mV. Fig. 11 shows an acute hippocampal slice on a 3D MEA and the responses evoked by stimulation of Schaffer collateral fibers. Stimulation of Schaffer collateral axons at the CA3/CA1 border or in the CA1 region evoked large responses in the pyramidal cell layer of the CA1 region. On the other hand, stimulation of the dentate gyrus generated generally smaller responses in the CA3 region via the mossy fiber pathway (data not shown here).

3.6. 3D versus planar electrode arrays

I/O curves of evoked responses were used to compare planar and 3D electrodes. The I/O curves were established by stimulating acute hippocampal slices with a current of increasing intensity (30–360 μA with 30 μA steps, see Section 2). Fig. 11 shows a typical I/O curve experiment. Three recordings of the same stimulation protocol were made with a delay of 10 min between the measurements. No important variations of the signal shape and amplitude occurred during the three I/O curve measurements. Experimental results obtained with planar ($n = 10$) and 3D ($n = 10$) MEA demonstrate that the amplitudes of evoked responses obtained with 3D MEA are larger than those obtained with planar MEA (Fig. 12a). A gain in amplitude of evoked population spikes between a factor 2.2 and 2.4 was achieved during these experiments. However, this gain is mainly due to the increased electrode area when using 3D electrodes. The advantage of the electrode geometry can be seen when normalizing the same data against 100% of the signal amplitude (Fig. 12b). In this case, a shift to lower stimulation currents of the input/output relation for the 3D electrodes can be seen. About 25% less current was necessary to obtain 50% of the maximum signal amplitude when using 3D instead of planar stimulation and recording electrodes. One possible explanation of this result is that a more local stimulation occurred due to the tip geometry and that there

is a shorter distance between the cells and the electrodes. In addition, the distribution of the largest peak-to-peak signal amplitudes ($n = 190$, corresponds approximately to 10 electrodes taken into account for each experiment) of planar ($n = 10$) and 3D ($n = 10$) experiments shows a shift to larger amplitudes (Fig. 12c), suggesting a global effect due to the different electrical and geometrical characteristics of the planar and 3D electrodes.

Although this approach is very useful in real experiments, it mixes the effects of the different surface areas of the stimulation electrodes with that of the recording efficacy of the electrodes. If a 3D electrode would recruit effectively all available fibers close to the electrode at low stimulus strengths, due to an increased stimulation efficacy, increasing the stimulus current would lead to a faster saturation than for planar electrodes. This could also be an explanation of the results shown in Fig. 12b. To access the differ-
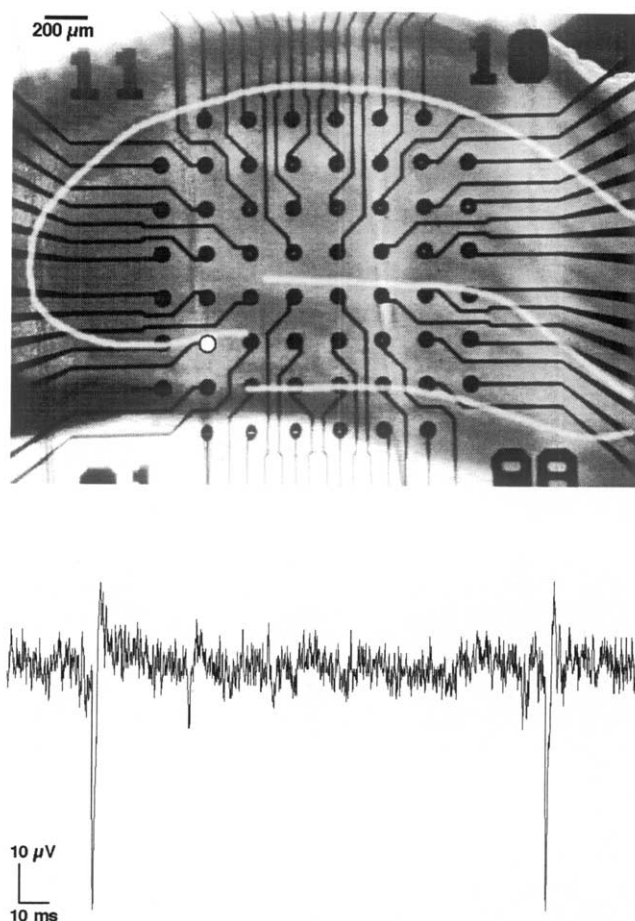

Fig. 10. Top, picture of an acute rat hippocampus slice on a 3D MEA held in place using a nylon mesh. The white lines represent schematically the CA1/CA3 region (upper line) and the dentate gyrus (lower lines). Bottom, an example of single-unit extracellular action potential recorded from a pyramidal neuron lying above one electrode located in the CA3 region (white dot). Under such conditions, it is possible to record spontaneous single extracellular action potentials from pyramidal neurons in both the CA3 and CA1 region (not shown here).
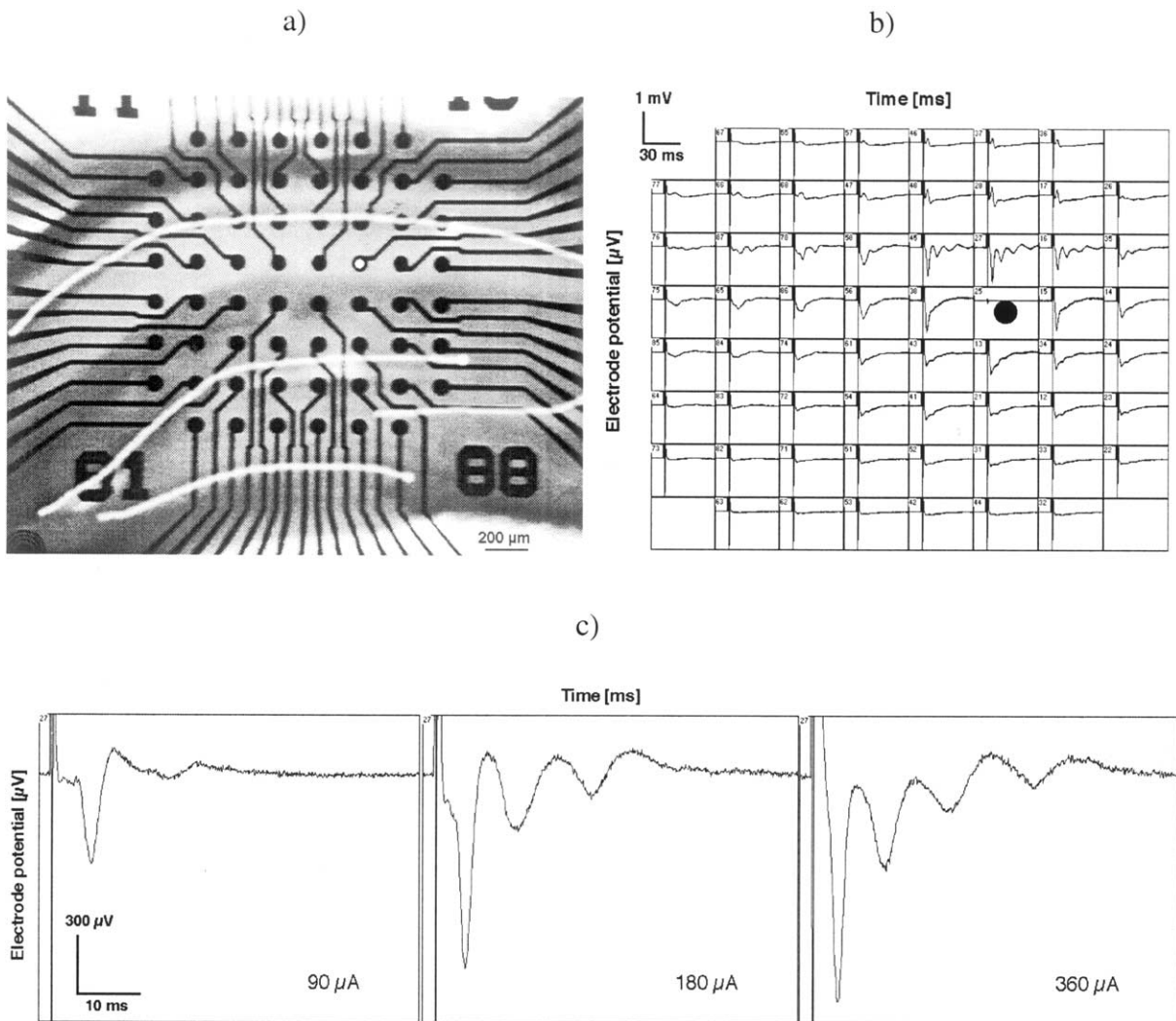
Fig. 11. Recording of field potentials in an acute hippocampal slice. A slice was placed onto the electrodes (no nylon mesh was necessary to hold the slice in place) and current pulses were applied through one MEA electrode to locally stimulate the slice. The other electrodes were used for extracellular recording of electrical activity in the slice. (a) Picture of a hippocampal slice on a 3D MEA. The stimulation electrode is shown in white. (b) Responses evoked in the shown hippocampal slice by $-/+$ 360 μA, 120 μs lasting stimulation pulse on Schaffer collateral fibers in the CA1 region (black dot). In each case, the signal collected at the corresponding electrode is represented. (c) Evoked responses obtained at the electrode above the stimulation electrode (case no. 27) located in CA1 region, 200 μm away stimulation electrode, when applying $-/+$ current pulses having amplitudes of 90, 180 and 360 μA, respectively, and lasting 120 μs. Note that the evoked population spike was multiple.

ence attributable to the stimulation versus recording conditions, a supplementary experiment using an external stimulation electrode was done. A glass theta microelectrode was used to stimulate acute slices from the top when recordings were made either with planar or 3D MEA. To minimize experimental variation, the same slice was used first on a planar electrode array and then onto a 3D MEA. Positioning of the slice was made as accurately as possible on the two arrays in order to insure the most comparable conditions. The obtained maximum peak-to-peak amplitudes at saturation from six experiments in which the slice has been placed onto a 3D electrode with a precision of $\pm$ 30 μm are shown in Fig. 13. It appears that the amplitude increase shown in Fig. 12a was not verified. However, it

turned out to be not significant under these experimental conditions, since the obtained amplitudes variation varied between a factor of 0.97 and a factor of 1.99 with a mean value of 1.29 over the six experiments. Given that the slice may have suffered from being transferred to a different MEA this could be the reason for not having a significant advantage of the 3D MEA in this situation. Nevertheless, the responses obtained with the 3D MEA appeared to be larger. However, when the I/O curves were plotted against 100% of the signal amplitude, there remained no clear advantage of the 3D electrodes as shown in Fig. 12b (not shown here). This suggests that with the current size of the 3D electrodes, the main advantage might reside in the stimulation efficacy.
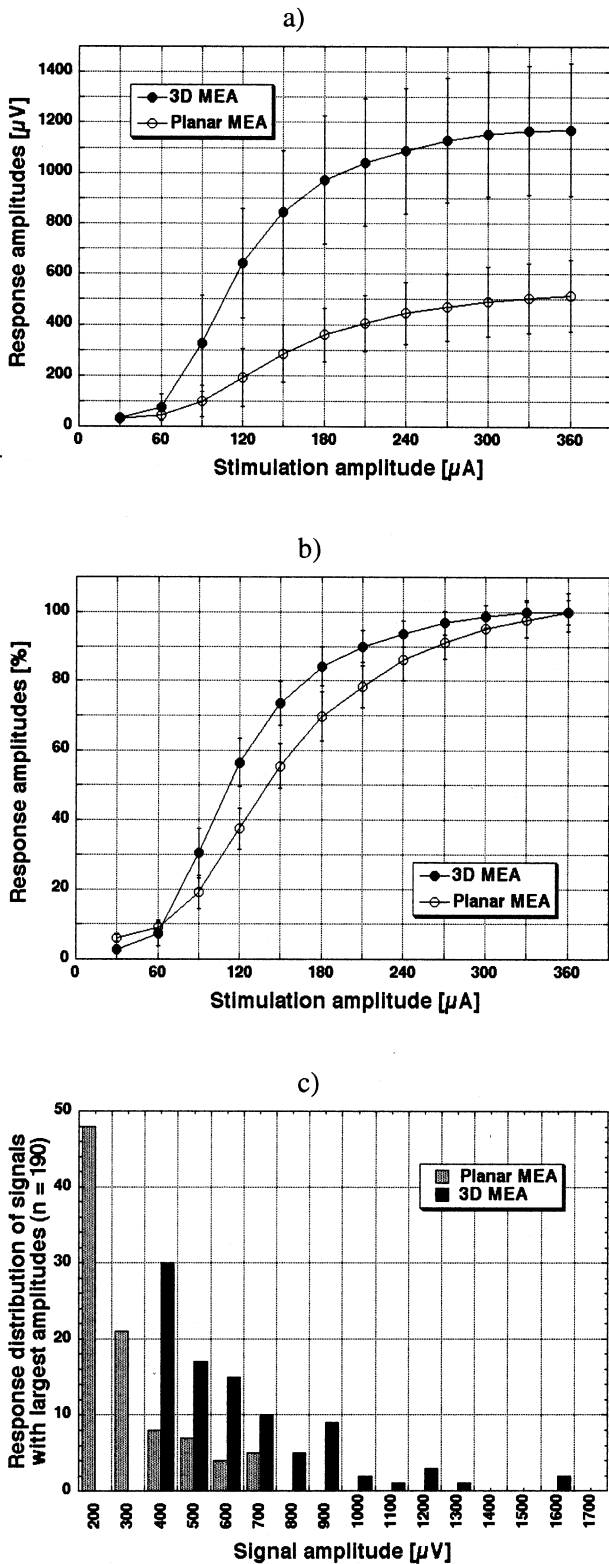
under standard experimental conditions (see Section 2). Stimulation was carried out every 30 s with biphasic current pulses (− / + 200 μA amplitudes, lasting 120 μs). The population spike peak-to-peak amplitudes were calculated for each stimulation pulse on several electrodes. As shown in Fig. 14, the signals from long-term experiments with planar and 3D MEA did not vary in shape or in amplitude. The variation over time of population spike peak-to-peak amplitude was less than 20% of the amplitude mean value. These results demonstrate that persistent stable conditions remained during the experiments.

Fig. 12. (a) Mean values of the largest population spike amplitude responses obtained with planar ($n = 10$) and 3D ($n = 10$) MEA as a function of current stimulation amplitudes. For the largest stimulation amplitude, a gain of 2.27 is obtained with the 3D electrode compared to planar electrode recordings. This gain can be explained by the increase of the 3D-electrode surface. (b) Same results as in (a) but plotted against the normalized signal amplitude. The results obtained with 3D MEA show a shift to the left compared to planar electrodes. One possible explanation is that the active cells are closer to the 3D electrodes than in a planar electrode configuration. (c) Distribution of signals showing the largest peak-to-peak signal amplitudes ($n = 190$, corresponds approximately to 10 electrodes taken into account for each experiment) of planar ($n = 10$) and 3D ($n = 10$) MEA as a function of the signal amplitude. Signals obtained with 3D MEA show a shift to the right, i.e. to larger response amplitudes with a gain between 2 and 2.3.
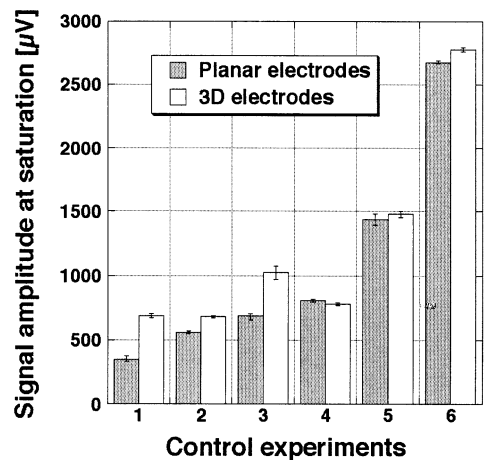
Fig. 12.

Fig. 13. Results of a control experiment using the extremity of a theta glass electrode for stimulation (diameter of 50 μm). Largest signal amplitudes obtained in six different experiments, in which a slice was first placed onto a planar MEA and then placed under the same conditions (placement error about ± 30 μm) onto a 3D MEA. The recorded signal amplitudes at saturation show no significant advantage of the 3D electrodes in this case, even when the normalized signal amplitude is plotted (not shown here). Note, however, that signals obtained using the 3D MEA appear to be larger.

3.7. Stability of evoked responses

Stability of evoked population spike responses was tested on planar and 3D MEA over time periods of 1 h
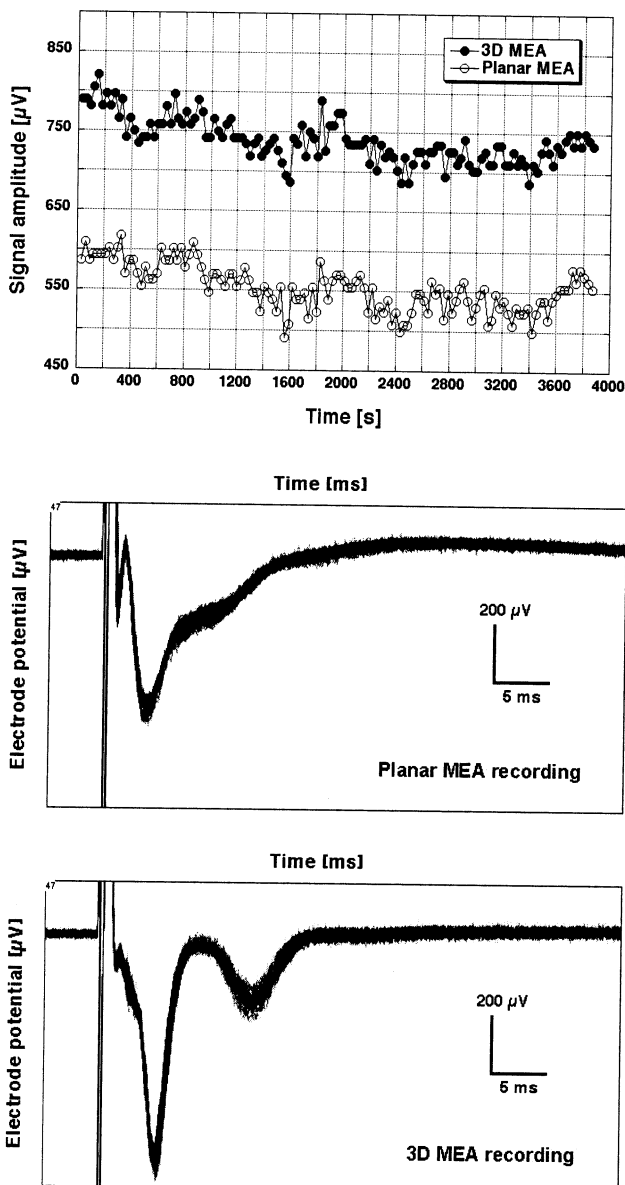
Fig. 14. Long-term signal stability experiment. Top, illustration of the stability of the response amplitude measured in the CA1 region over a time period of more than 1 h for a ($-/+$) 200 μA, 120 μs current pulse delivered every 30 s for both a planar and a 3D MEA. Bottom, superposition of all population spikes obtained at the electrode showing the largest signal amplitude in this experiment. The population spikes obtained with the 3D MEA show a steeper signal slope, indicating that in this case the active neurons are closer to the recording electrodes.

4. Conclusions

Although intracellular measurements have provided an incredibly sharp picture of the neuronal activity at a single cell level, multiple recordings using microelectrodes are reaching a technical limit and new techniques need to be developed to satisfy the growing interest of neuronal network investigation. Organotypic tissue cultures are widely used to get an insight into neural networks. However, the natural connectivity between the neurons may be lost after a few days in culture due to a different cell-to-cell connectivity. On the other hand, the use of acute tissue slices allows to obtain an insight into a reduced natural network. The dead cell layers at the tissue slice border reduces the measurable signal amplitudes and limits the signal. In this paper, we propose the use of 3D electrode arrays to allow better monitoring conditions due to an increase of the electrode area, reducing the overall electrode impedance, and due to the tissue penetration allowing to be closer to the active cells in the preparation.

Further, the development of this 3D MEA as a single-use low-cost item is in progress, making this new tool accessible to the basic researcher and the pharmaceutical industry.

References

Gross GW, Rieske E, Kreutzberg GW, Meyer A. A new fixed-array multi-microelectrode system designed for long-term monitoring of extracellular single unit neuronal activity in vitro. Neurosci Lett 1977;6:101–5.

Lorenz H, Despont M, Fahrni N, LaBianca N, Renaud P, Vettiger P. SU-8: a low-cost negative resist for MEMS. J Micromech Microeng 1997;7:121–4.

Lorenz H, Despont M, Fahrni N, Brugger J, Vettiger P, Renaud P. High-aspect-ratio, ultrathick, negative-tone near-UV photoresist and its applications for MEMS. Sensors Actuators A 1998;64:33–9.

Madou M. Fundamentals of microfabrication. New York: CRC Press, 1997:589.

Novak JL, Wheeler BC. Multisite hippocampal slice recording and stimulation using a 32 element microelectrode array. J Neurosci Methods 1988;23:149–59.

Novak JL, Wheeler BC. Two-dimensional current source density analysis of propagation delays for components of epileptiform bursts in rat hippocampus slices. Brain Res 1989;497:223–30.

Oka H, Shimono K, Ogawa R, Sugihara H, Taketani M. A new planar multielectrode array for extracellular recording: application to hippocampal acute slice. J Neurosci Methods 1999;93:61–7.

Rai-Choudhury P. Handbook of Microlithography, Micromachining and Microfabrication. Bellingham: SPIE Press, 1997:670.

Rall W. Electrophysiology of a dendritic neuron model. Biophy J 1962;2:145–67.

Thiébaud P, de Rooij NF, Koudelka-Hep M, Stoppini L. Microelectrode arrays for electrophysiological monitoring of hippocampal organotypic slice cultures. IEEE Trans Biomed Eng 1997;44:1159–63.

Thiébaud P, Beuret C, Koudelka-Hep M, Bove M, Martinoia S, Grattarola M, Jahnsen H, Rebaudo R, Balestrino M, Zimmer J, Dupont Y. An array of Pt-tip microelecrodes for extracellular monitoring of activity of brain slices. Biosens Bioelectron 1999;14:61–5.

Thomas CA, Springer PA, Loeb GE, Berwald-Netter Y, Okun LM. A miniature microelectrode array to monitor the bioelectric activity of cultured cells. Exp Cell Res 1972;74:61–6.

Wheeler BC, Novak JL. Current source density estimation using microelectrode array data from the hippocampal slice preparation. IEEE Trans Biomed Eng 1986;33:1204–12.